Applied Physics Letters

Robust waveguiding in substrate-integrated topological photonic crystals

Cite as: Appl. Phys. Lett. **116**, 231106 (2020); https://doi.org/10.1063/5.0003888
Submitted: 05 February 2020 . Accepted: 27 May 2020 . Published Online: 12 June 2020

Qiaolu Chen, Li Zhang, Su Xu, Zuojia Wang, Erping Li, Yihao Yang, and Hongsheng Chen

View Online Export Citation CrossMark

ARTICLES YOU MAY BE INTERESTED IN

Size-tunable electroluminescence characteristics of quantum confined Si nanocrystals embedded in Si-rich oxide matrix
Applied Physics Letters **116**, 231105 (2020); https://doi.org/10.1063/5.0001840

Superconducting quantum many-body circuits for quantum simulation and computing
Applied Physics Letters **116**, 230501 (2020); https://doi.org/10.1063/5.0008202

The quantum future of microscopy: Wave function engineering of electrons, ions, and nuclei
Applied Physics Letters **116**, 230502 (2020); https://doi.org/10.1063/1.5143008

Lock-in Amplifiers up to 600 MHz
Watch

AIP Publishing

© 2020 Author(s).

Applied Physics Letters ARTICLE scitation.org/journal/apl

Robust waveguiding in substrate-integrated topological photonic crystals

Cite as: Appl. Phys. Lett. **116**, 231106 (2020); doi: 10.1063/5.0003888
Submitted: 5 February 2020 · Accepted: 27 May 2020 ·
Published Online: 12 June 2020

View Online Export Citation CrossMark

Qiaolu Chen,[1,2] Li Zhang,[1,2] Su Xu,[3] Zuojia Wang,[4] Erping Li,[1] Yihao Yang,[5,6,a)] and Hongsheng Chen[1,2,a)]

AFFILIATIONS

[1]Key Lab. of Advanced Micro/Nano Electronic Devices and Smart Systems of Zhejiang, Zhejiang University, Hangzhou 310027, China
[2]The Electromagnetics Academy at Zhejiang University, College of Information Science and Electronic Engineering, Zhejiang University, Hangzhou 310027, China
[3]State Key Laboratory of Integrated Optoelectronics, College of Electronic Science and Engineering, Jilin University, 2699 Qianjin Street, Changchun 130012, China
[4]Z. Wang is with School of Information Science and Engineering, Shandong University, Jinan 250100, China
[5]Division of Physics and Applied Physics, School of Physical and Mathematical Sciences, Nanyang Technological University, 21 Nanyang Link, Singapore 637371, Singapore
[6]Centre for Disruptive Photonic Technologies, The Photonics Institute, Nanyang Technological University, 50 Nanyang Avenue, Singapore 639798, Singapore

[a)]**Authors to whom correspondence should be addressed:** yang.yihao@ntu.edu.sg and hansomchen@zju.edu.cn

ABSTRACT

Recent development of topological photonics has enabled photonic energy flow robust against disorders. On the other hand, waveguiding in substrate-integrated planar platforms is significant for microwave and mm-wave technology. Here, we propose substrate-integrated topological photonic crystals (PhCs) that support robust pseudospin-dependent edge states. We verify the robustness of pseudospin-dependent electromagnetic-wave (EM-wave) energy transport through sharply twisted corners, random defects, or a channel intersection both numerically and experimentally at microwave frequencies. The present topological PhCs with planar forms, small thicknesses, and excellent electrical shielding pave the way toward manipulation of EM topological pseudospins in an integrated platform.

Published under license by AIP Publishing. https://doi.org/10.1063/5.0003888

Over the last decade, motivated by topological physics in condensed matter systems, researchers have proposed and realized different kinds of topological photonic crystals (PhCs),[1–4] whose bulks are opaque, while edges support one-way chiral or pseudospin-polarized helical edge states that arise from the non-trivial band topology. Such topological photonic edge states are backscattering-immune and robust against defects and disorders. The study of topological PhCs has revealed a variety of promising applications, such as high-efficiency waveguiding,[5] robust optical delay lines,[6] topological channel intersections,[7–9] and topological lasers.[10–12]

Based on different physical effects, the topological PhCs can be classified into several categories, including time-reversal-broken quantum-Hall topological PhCs,[5,13–15] time-reversal-preserved spin-Hall topological PhCs,[7,16–26] and inversion-broken valley-Hall topological PhCs.[8,9,27–35] As the quantum-Hall topological PhCs usually require gyromagnetic materials in a uniform magnetic field or complicated temporal modulation[5,36,37] to break the time-reversal symmetry, which is experimentally challenging, we here focus on the time-reversal-preserved counterparts. In addition, while the topological properties of valley-Hall topological PhCs arise from local Berry curvatures near valleys in momentum space and the global Chern or spin-Chern numbers of their bulk bands are zero,[33] the topological features of spin-Hall topological PhCs are characterized by zero global Chern numbers but non-zero global spin-Chern numbers, which result in the robust topological edge states against various disorders, such as defects, lattice disorders, and sharp corners with arbitrary bending angles.[18–20,23,24] In this work, we mainly focus on spin-Hall topological PhCs.

One way to design the spin-Hall topological PhCs is to take advantage of electromagnetic (EM) duality.[7,16,17,21,26] Such topological PhCs are usually obtained by introducing bi-anisotropy into a system, where transverse electric (TE) and transverse magnetic (TM) Dirac points are degenerate via fine tuning. Applying the crystalline symmetry is another way to design the spin-Hall topological PhCs.[18–20,22–25]

Published under license by AIP Publishing

For example, Wu and Hu proposed a topological PhC purely based on dielectric materials, where the topological photonic states are protected by pseudo-time-reversal symmetry that is a combination of time-reversal symmetry determined by Maxwell equations and C_6 crystalline symmetry.[18]

For microwave and mm-wave technology, achieving waveguides with a high quality factor, high power-handling capability, excellent electrical shielding, ease of fabrication, low cost, and planar form is of fundamental importance. This has motivated the development of the substrate-integrated waveguide (SIW) technique that has been widely adopted in microwave engineering.[38–41] The SIWs have many characteristics and merits that are similar to those of the rectangular waveguides, such as mode patterns and dispersion relations of guided modes. In addition to the merits inheriting from rectangular waveguides, the SIWs have particular advantages, such as compatibility with the standard printed circuit board (PCB) technique, easy access, and low cost. Therefore, the SIWs offer the possibility to integrate several kinds of passive and active components, such as waveguide splitters,[7–9] filters,[42,43] amplifiers,[44] and antennas[41,45] into one platform.

In this work, inspired by the SIW technique, we propose and experimentally realize substrate-integrated topological PhCs based on the photonic analog of the quantum spin-Hall effect guaranteed by the C_6 crystalline symmetry and time-reversal symmetry at microwave frequencies. In comparison to the conventional spin-Hall topological PhCs at microwave or mm frequencies,[7,16,20,22,24,26] the proposed substrate-integrated topological PhCs have plenty of merits, such as high confinement of EM waves in the vertical direction to prevent radiation from leaking into free space, excellent electrical shielding, small thicknesses, planar geometry, and good compatibility with the PCB technique and conventional SIW circuits. By interfacing two substrate-integrated PhCs with distinct topologies, we construct a domain wall where topologically pseudospin-dependent edge states propagate with negligible backscattering and high efficiency, even in the presence of sharp turns or arbitrary defects. Besides, topologically pseudospin-dependent transport is realized in a topological channel intersection.

The fabricated substrate-integrated PhC is shown in Fig. 1(a). The PhC is in a triangular lattice with a lattice constant of $a = 21$ mm and is arranged in a parallel waveguide that is loaded with a dielectric material with a relative permittivity of $\varepsilon = 2.55$ [see Figs. 1(a) and 1(b)]. Figure 1(c) shows the details of a unit cell, where a metallic mesh pattern is placed between two parallel plates and a gap with a size of $g_0 = 0.5$ mm is between the metallic mesh pattern and the top plate. The metallic mesh pattern contains six triangles with a side length of $l = 6.53$ mm, which are located at six corners of a hexagon with side length R. In our work, topological phase transition is controlled by varying R. The adjacent triangles are connected via metallic wires with a width of $w = 1.21$ mm. The metallic cylinders with a height of $h = 3.2$ mm and a radius of $r_0 = 1.17$ mm are utilized to connect the metallic mesh patterns to the bottom plate.

In the experiment, our sample is composed of two PCBs. The metallic mesh patterns and via holes are printed on the bottom PCB [see Fig. 1(a)]. The top PCB provides a gap and is attached on the bottom PCB with an adhesive. The experimental sample has a small thickness of 3.7 mm (i.e., $0.14^{*}\lambda_1$, where λ_1 is the wavelength of the EM wave in our dielectric material) and is sandwiched between two 35-μm parallel copper plates, which confine the light in the vertical direction and could provide a compatible platform with conventional SIW circuits.

We first consider a PhC with $R = 7.00$ mm, whose band structure is shown in Fig. 2(a). Note that the numerical dispersions and the corresponding eigenmodes of the bulk states are obtained by employing the eigenvalue module of the commercial software COMSOL Multiphysics. One can see that the band structure possesses a doubly degenerate Dirac point at the Γ point in the Brillouin zone at the frequency of 6.90 GHz. When slightly decreasing R to 5.74 mm [PhC1, the corresponding band structure and geometry are shown in Fig. 2(b)] or increasing R to 7.84 mm [PhC2, the corresponding band structure and geometry are shown in Fig. 2(c)], the Dirac point splits, and hence, a complete bandgap opens. Although the band structures of PhC1 and PhC2 look similar, their band topologies are completely distinct. In order to analyze the band topologies, we check the modes at the Γ point. For the case of $R = 5.74$ mm, there are two pairs of degenerate modes below/above the bandgap, whose E_z field distributions are shown in Fig. 2(d). We find that there are two dipole modes denoted as p states below the bandgap and two quadrupole modes denoted as d states above the bandgap. Interestingly, for the case of $R = 7.84$ mm, the modes below and above the bandgap are inverted [see Fig. 2(e)], i.e., p/d states are above/below the bandgap, revealing a band inversion phenomenon that is the signature of topological phase transition.[18]

We would like to mention that, because the height of our parallel waveguide (3.7 mm) is much smaller than the cutoff wavelength of TE

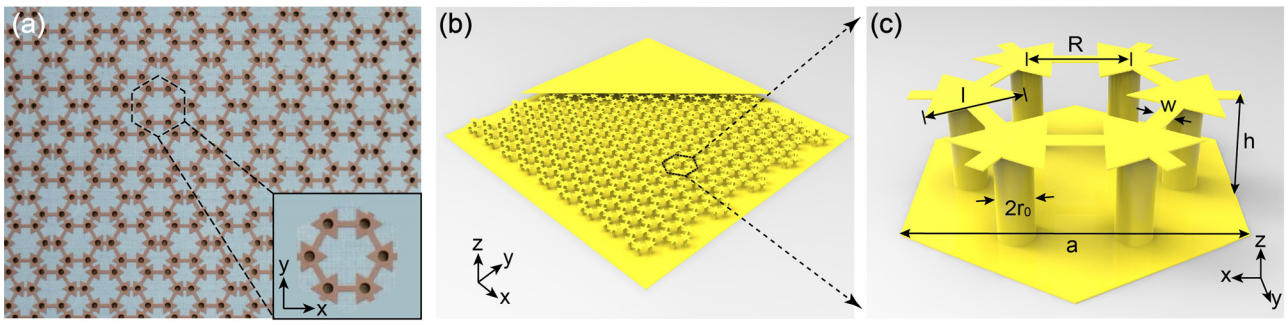

FIG. 1. (a) Perspective-view photograph of an experimental sample fabricated via the PCB technique. The black dashed hexagonal line depicts a unit cell. Inset: enlarged view of a unit cell. (b) Periodically arranged PhCs in a triangular lattice. The dashed black hexagonal line labels a unit cell. (c) Enlarged view of a unit cell. Here, $a = 21$ mm, $r_0 = 1.17$ mm, $h = 3.2$ mm, $l = 6.53$ mm, and $w = 1.21$ mm. The thickness of the metal layer is 0.035 mm.

Published under license by AIP Publishing

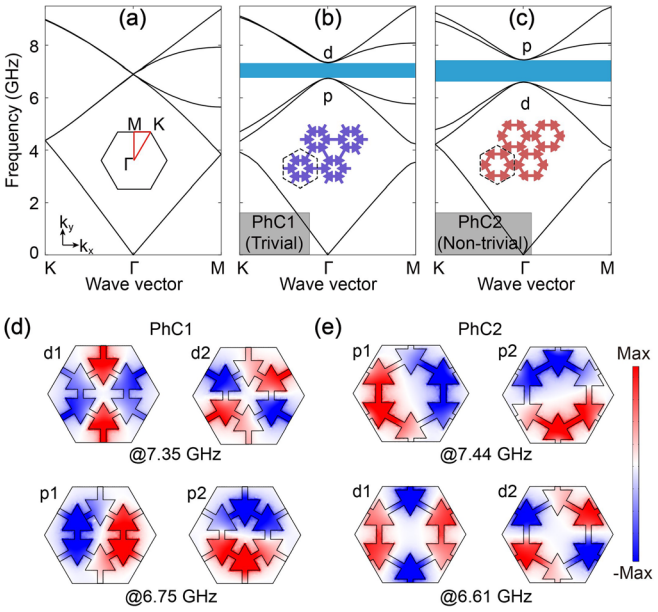

FIG. 2. (a) Band structure for the PhC with $R = 7.00$ mm. Inset: the first Brillouin zone of the triangular lattice. (b) and (c) Band structures for PhC1 (blue) with $R = 5.74$ mm and PhC2 (red) with $R = 7.84$ mm, respectively. Blue areas represent the bandgaps. (d) and (e) Simulated E_z field patterns of *p* and *d* states at the Γ point on the $z = -0.1$ mm plane, which correspond to the four bands (*p1*, *p2*, *d1*, and *d2*) observed in the band structures of PhC1 and PhC2, respectively.

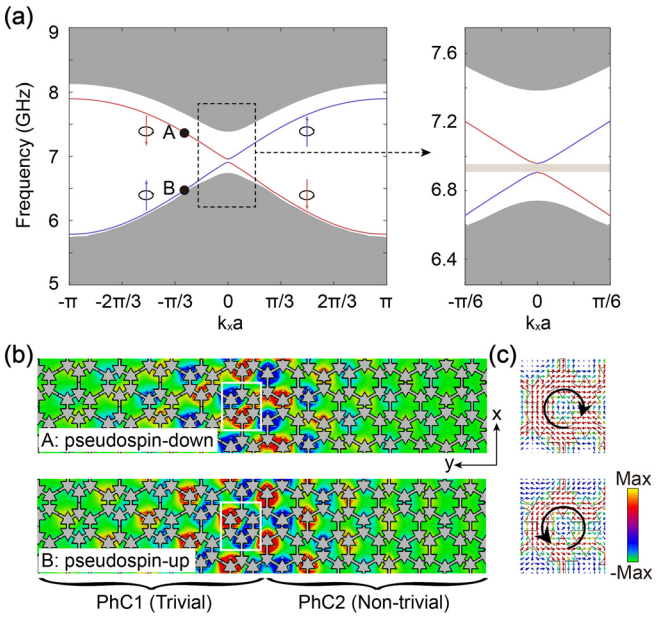

FIG. 3. (a) Dispersion relations of the domain wall. Red (blue) lines are for pseudospin-down (pseudospin-up) edge states, and shaded areas are for projected bulk states. Right panel: enlarged view of (a). There is a tiny gap at $k_x = 0$. (b) Real-space distributions of the E_z field at A and B points labeled in (a). (c) Time-averaged Poynting vectors in a PhC1, which are depicted by a white rectangle in (b), associated with the pseudospin-down (A point) and pseudospin-up (B point) edge states.

modes (approximately 22 mm), only TM modes with an out-of-plane electric field survive below 8.00 GHz. Thus, we here focus on the TM modes with an out-of-plane electric field and an in-plane magnetic field. Therefore, our design is different from previous spin-Hall topological PhCs in meta-waveguides based on the EM duality that involves both TE and TM modes.[17]

Then, we construct a domain wall consisting of trivial PhC1 ($R = 5.74$ mm) and topological non-trivial PhC2 ($R = 7.84$ mm) in the *y* direction. By sweeping k_x from $-\pi/a$ to π/a, the dispersion relations of the domain wall are calculated numerically, as shown in Fig. 3(a), where shaded areas represent the projection of bulk states. One can see that a pair of edge states marked as red and blue lines appears within the bandgap. We check the real-space distributions of the E_z field at A and B points, as shown in Fig. 3(b), which indicate that the in-gap states are highly located around the domain wall, thus revealing the existence of topological edge states. We also plot the real-space distributions of the time-averaged Poynting vectors at A and B points, as shown in Fig. 3(c). The Poynting vectors show vortex structures, indicating the existence of pseudospin-up or pseudospin-down states depending on the direction of the Poynting vectors. Note that there is a small gap at $k_x = 0$ as shown in the right panel of Fig. 3(a). This is because C_6 crystalline symmetry is reduced at the edges of the structure, and thus, the pseudo-time-reversal symmetry would cause scattering and mixing between the two pseudospins as in other spin-Hall topological PhCs (see the supplementary material).[18] This also implicates that the topological protection is slightly reduced (not as strong as that in Z_2 electronic topological insulators where the topological states are protected by the Fermionic time-reversal symmetry). Therefore, the topological edge states are not strictly immune to backscattering, as in time-reversal systems, photonic pseudospins can always couple to each other owing to reciprocity (see the supplementary material).[46] Nevertheless, the backscattering of the topological edge states is still suppressed as long as the edge states are not embedded into the bulk states.

The topological edge states have been proven to be robust against sharply twisted corners or random defects, due to the strong suppression of the backscattering.[20,24] To experimentally demonstrate their nature and robustness of topological protection, we set up an experiment, as shown in Fig. 4(a), where a vector network analyzer (VNA) collects transmission from port 1 and port 2. Two vertical dipole antennas oriented along the *z* direction, acting as a source and a probe, are placed inside the designed waveguides at port 1 and port 2 to excite and receive EM waves at the frequencies within the topological bandgap, respectively.

Four samples are manufactured by employing the PCB technique, including a sample without a domain wall, a straight domain wall, a Z-shape domain wall, and a straight domain wall decorated with random disorders. The straight domain wall is composed of PhC1 (on the left side) and PhC2 (on the right side) [Fig. 4(c)]. The Z-shape domain wall consists of two 120° turns [Fig. 4(d)]. The domain wall with random disorders is similar to the straight one except for the impurity in the right region (i.e., 8 PhC2 on the right side are replaced by 8 PhC1 randomly), as shown in Fig. 4(e).

Figure 4(b) shows the measured transmissions for edge states along the straight/Z-shape/disordered domain walls (blue/red/yellow

Published under license by AIP Publishing

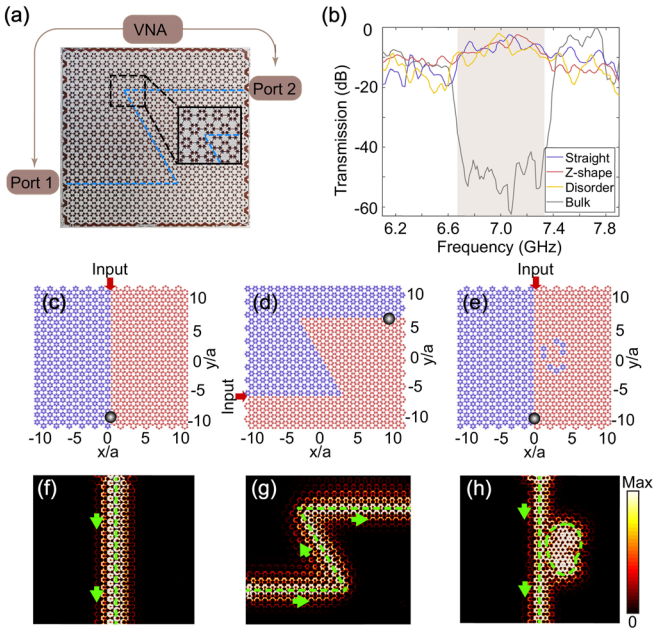

FIG. 4. (a) Experimental setup for the transmission measurement. The blue dashed line indicates the Z-shape domain wall. The inset shows a zoomed-in photograph. (b) Measured normalized transmissions for topological edge states along the straight/Z-shape/disordered domain walls (blue/red/yellow lines) and for bulk states along the sample without the domain wall (gray line). The region highlighted in gray indicates the bulk bandgap. All transmissions are normalized to the maximum value of the bulk transmission. (c)–(e) Cross-sectional schematic views of a straight domain wall, a Z-shape domain wall, and a domain wall decorated with random disorders, respectively. The blue (red) unit cell represents PhC1 (PhC2). Red arrows: point sources. Black dots: detectors. (f)–(h) Distributions of simulated electric field intensity at 7.2 GHz corresponding to (c)–(e), respectively. Green arrows depict the propagating direction of topological energy transport.

lines) and for bulk states along the sample without the domain wall (gray line). We observe an obvious 40-dB drop in the transmission of bulk states, which reveals a bandgap extending from approximately 6.65 GHz–7.35 GHz. The transmission of the Z-shape domain wall is close to that of the straight domain wall. Both of them remain high within the frequency range of the bandgap, indicating the existence of topological edge states. Besides, the transmission of the domain wall with random disorders is found to be disorder-insensitive and comparable to the transmission of the previous straight domain wall. Thus, the measured transmissions verify the robustness of topologically pseudospin-dependent EM-wave energy transport through sharply twisted corners and random defects.

To show how the topological edge states propagate through different disorders, we implement full-wave simulations in the time domain of CST Microwave studio on these three designed domain walls, respectively [see Figs. 4(c)–4(e)]. Figures 4(f)–4(h) illustrate the distributions of simulated electric field intensity of topological edge states propagating along the three domain walls at 7.2 GHz, where the green arrows represent the propagating direction of topological edge states. One can see that the EM energy is strongly confined at the domain walls for all three cases, especially the edge states smoothly pass through two 120° corners [see Fig. 4(g)] and disordered cavity [see Fig. 4(h)] with highly suppressed backscattering and reflections. Note that such propagation is also valid for other frequencies inside the bandgap, which could lead to photonic broadband operation. Therefore, it is clear that the simulated results are consistent with the experimental observations, confirming the robustness and topological protection of the edge states.

To further confirm the pseudospin-dependent edge states, a topological channel intersection is designed and its schematic view is shown in Fig. 5(a). The topological channel intersection is composed of four domains with four ports labeled as 1–4 at the terminals of four paths. The topologically pseudospin-dependent edge states supported by four paths are shown in Fig. 5(a), where the red (blue) arrows represent pseudospin-up (-down) states. Figures 5(b) and 5(c) illustrate the distributions of simulated electric field intensity at 7.2 GHz when placing a point source at port 1 and port 4, respectively. One can see that the EM waves at port 1 (port 4) can only propagate to port 2 and port 4 (port 1 and port 3).

In the experiments, a source antenna is placed at port 1 (port 4), while probe antennas are placed at the remaining three ports. The experimental results shown in Figs. 5(d) and 5(e) are consistent with simulated results. These results indicate that the edge transports involving different pseudospins [S31 in Fig. 5(d) and S24 in Fig. 5(e)] are strongly suppressed compared to those involving the same pseudospins [S21 and S41 in Fig. 5(d) and S14 and S34 in Fig. 5(e)] within the photonic bandgap frequency window (gray region). Thus, our experimental observation reveals that the photonic pseudospins are bound to the propagation of topological edge states at each path.

To conclude, we have proposed and experimentally demonstrated substrate-integrated spin-Hall topological PhCs. Topologically pseudospin-dependent edge states are observed at the domain wall between two PhCs with distinct band topologies. We show explicitly that the topological EM-wave energy propagates along sharply twisted corners, disordered paths, or a channel intersection with strongly suppressed backscattering and reflections. Our designed topological PhCs

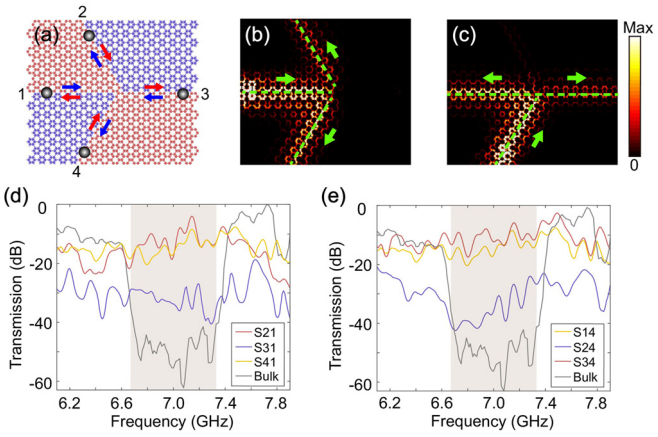

FIG. 5. (a) Cross-sectional schematic view of a topological channel intersection. The blue (red) unit cell: PhC1 (PhC2). Black dots: point sources. Red (blue) arrows: pseudospin up (down). (b) and (c) Distributions of simulated electric field intensity at 7.2 GHz when placing a point source at port 1 (b) and port 4 (c), respectively. Green arrows depict the propagating direction of topological energy transport. (d) and (e) Measured normalized transmissions when placing a point source at port 1 (d) and port 4 (e). The region highlighted in gray indicates the bulk bandgap. All transmissions are normalized to the maximum value of the bulk transmission.

Published under license by AIP Publishing

in a planar form have advantages of small thicknesses, light weight, disorder insensitivity, self-consistent electrical shielding, and good compatibility with the PCB technique and conventional SIW circuits, which provide a pathway to manipulate EM pseudospins in an integrated platform.

See the supplementary material for the relationship between the reduction of C_6 symmetry and the destruction of topologically protected transport.

The work at Zhejiang University was sponsored by the National Natural Science Foundation of China (NNSFC) under Grants Nos. 61625502, 11961141010, and 61975176, the Top-Notch Young Talents Program of China, and the Fundamental Research Funds for the Central Universities. The work at Nanyang Technological University was sponsored by the Singapore Ministry of Education under Grant Nos. MOE2018-T2-1-022 (S), MOE2015-T2-1-070, MOE2016-T3-1-006, and Tier 1 RG174/16 (S).

DATA AVAILABILITY

The data that support the findings of this study are available from the corresponding author upon reasonable request.

REFERENCES

[1]L. Lu, J. D. Joannopoulos, and M. Soljačić, Nat. Photonics **8**, 821 (2014).
[2]L. Lu, J. D. Joannopoulos, and M. Soljačić, Nat. Phys. **12**, 626 (2016).
[3]A. B. Khanikaev and G. Shvets, Nat. Photonics **11**, 763 (2017).
[4]T. Ozawa, H. M. Price, A. Amo, N. Goldman, M. Hafezi, L. Lu, M. C. Rechtsman, D. Schuster, J. Simon, O. Zilberberg, and I. Carusotto, Rev. Mod. Phys. **91**, 015006 (2019).
[5]Z. Wang, Y. Chong, J. D. Joannopoulos, and M. Soljačić, Nature **461**, 772 (2009).
[6]M. Hafezi, E. A. Demler, M. D. Lukin, and J. M. Taylor, Nat. Phys. **7**, 907 (2011).
[7]X. Cheng, C. Jouvaud, X. Ni, S. H. Mousavi, A. Z. Genack, and A. B. Khanikaev, Nat. Mater. **15**, 542 (2016).
[8]X. Wu, Y. Meng, J. Tian, Y. Huang, H. Xiang, D. Han, and W. Wen, Nat. Commun. **8**, 1304 (2017).
[9]L. Zhang, Y. Yang, M. He, H.-X. Wang, Z. Yang, E. Li, F. Gao, B. Zhang, R. Singh, J.-H. Jiang, and H. Chen, Laser Photonics Rev **13**, 1900159 (2019).
[10]B. Bahari, A. Ndao, F. Vallini, A. E. Amili, Y. Fainman, and B. Kanté, Science **358**, 636 (2017).
[11]M. A. Bandres, S. Wittek, G. Harari, M. Parto, J. Ren, M. Segev, D. N. Christodoulides, and M. Khajavikhan, Science **359**, eaar4005 (2018).
[12]G. Harari, M. A. Bandres, Y. Lumer, M. C. Rechtsman, Y. D. Chong, M. Khajavikhan, D. N. Christodoulides, and M. Segev, Science **359**, eaar4003 (2018).
[13]F. D. M. Haldane and S. Raghu, Phys. Rev. Lett. **100**, 013904 (2008).
[14]S. Raghu and F. D. M. Haldane, Phys. Rev. A **78**, 033834 (2008).
[15]Z. Wang, Y. D. Chong, J. D. Joannopoulos, and M. Soljačić, Phys. Rev. Lett. **100**, 013905 (2008).
[16]W.-J. Chen, S.-J. Jiang, X.-D. Chen, B. Zhu, L. Zhou, J.-W. Dong, and C. T. Chan, Nat. Commun. **5**, 5782 (2014).
[17]T. Ma, A. B. Khanikaev, S. H. Mousavi, and G. Shvets, Phys. Rev. Lett. **114**, 127401 (2015).
[18]L.-H. Wu and X. Hu, Phys. Rev. Lett. **114**, 223901 (2015).
[19]S. Barik, H. Miyake, W. DeGottardi, E. Waks, and M. Hafezi, New J. Phys. **18**, 113013 (2016).
[20]S. Yves, R. Fleury, T. Berthelot, M. Fink, F. Lemoult, and G. Lerosey, Nat. Commun. **8**, 16023 (2017).
[21]A. Slobozhanyuk, S. H. Mousavi, X. Ni, D. Smirnova, Y. S. Kivshar, and A. B. Khanikaev, Nat. Photonics **11**, 130 (2017).
[22]Y. Li, Y. Sun, W. Zhu, Z. Guo, J. Jiang, T. Kariyado, H. Chen, and X. Hu, Nat. Commun. **9**, 4598 (2018).
[23]S. Barik, A. Karasahin, C. Flower, T. Cai, H. Miyake, W. DeGottardi, M. Hafezi, and E. Waks, Science **359**, 666 (2018).
[24]Y. Yang, Y. F. Xu, T. Xu, H.-X. Wang, J.-H. Jiang, X. Hu, and Z. H. Hang, Phys. Rev. Lett. **120**, 217401 (2018).
[25]M. L. N. Chen, L. J. Jiang, Z. Lan, and W. E. I. Sha, IEEE Trans. Antennas Propag. **68**, 609 (2020).
[26]Y. Yang, Z. Gao, H. Xue, L. Zhang, M. He, Z. Yang, R. Singh, Y. Chong, B. Zhang, and H. Chen, Nature **565**, 622 (2019).
[27]T. Ma and G. Shvets, New J. Phys. **18**, 025012 (2016).
[28]Z. Gao, Z. Yang, F. Gao, H. Xue, Y. Yang, J. Dong, and B. Zhang, Phys. Rev. B **96**, 201402 (2017).
[29]F. Gao, H. Xue, Z. Yang, K. Lai, Y. Yu, X. Lin, Y. Chong, G. Shvets, and B. Zhang, Nat. Phys. **14**, 140 (2018).
[30]J. Noh, S. Huang, K. P. Chen, and M. C. Rechtsman, Phys. Rev. Lett. **120**, 063902 (2018).
[31]M. I. Shalaev, W. Walasik, A. Tsukernik, Y. Xu, and N. M. Litchinitser, Nat. Nanotechnol. **14**, 31 (2019).
[32]X.-D. Chen, W.-M. Deng, J.-C. Lu, and J.-W. Dong, Phys. Rev. B **97**, 184201 (2018).
[33]X.-T. He, E.-T. Liang, J.-J. Yuan, H.-Y. Qiu, X.-D. Chen, F.-L. Zhao, and J.-W. Dong, Nat. Commun. **10**, 872 (2019).
[34]Q. Chen, L. Zhang, M. He, Z. Wang, X. Lin, F. Gao, Y. Yang, B. Zhang, and H. Chen, Adv. Opt. Mater. **7**, 1900036 (2019).
[35]Y. Yang, Y. Yamagami, X. Yu, P. Pitchappa, J. Webber, B. Zhang, M. Fujita, T. Nagatsuma, and R. Singh, Nat. Photonics (published online 2020).
[36]K. Fang, Z. Yu, and S. Fan, Nat. Photonics **6**, 782 (2012).
[37]K. Fang and Y. Wang, Phys. Rev. Lett. **122**, 233904 (2019).
[38]D. Deslandes and K. Wu, IEEE Microwave Wireless Compon. Lett. **11**, 68 (2001).
[39]F. Xu and K. Wu, IEEE Trans. Microwave Theory Tech. **53**, 66 (2005).
[40]D. Deslandes and K. Wu, IEEE Trans. Microwave Theory Tech. **54**, 2516 (2006).
[41]M. Bozzi, A. Georgiadis, and K. Wu, IET Microwave Antennas Propag. **5**, 909 (2011).
[42]X. Chen, W. Hong, T. Cui, J. Chen, and K. Wu, IEEE Microwave Wireless Compon. Lett. **15**, 787 (2005).
[43]X. Chen and K. Wu, IEEE Microwave Mag. **15**, 108 (2014).
[44]M. Abdolhamidi and M. Shahabadi, IEEE Microwave Wireless Compon. Lett. **18**, 815 (2008).
[45]M. Henry, C. E. Free, B. S. Izqueirdo, J. Batchelor, and P. Young, IEEE Trans. Adv. Packag. **32**, 93 (2009).
[46]B. Orazbayev and R. Fleury, Nanophotonics **8**(8), 1433 (2019).

Published under license by AIP Publishing